There may be differences between this version and the published version. You are advised to consult the publisher's version if you wish to cite from it.

http://eprints.gla.ac.uk/322535/

Deposited on 2 May 2024

**IEEE Sensors Council**

# Carbon Quantum Dot Embedding Silica–Molecularly Imprinted Polymer Coated Optical Fiber as Ratiometric Biosensors Toward Dopamine Detection

T. Azargoshasb, H. Ali Navid, S. Yadollahzadeh, R. Aghbolaghi, R. Parvizi, G-M. Parsanasab,

*Abstract*— **We have developed a ratiometric fluorescence sensor for detecting dopamine (DA) using a silica-based molecular imprinting polymer (MIP) coated on cabbage-derived blue emissive carbon quantum dot (CQD) and deposited on optical fiber. Physicochemical characterization confirmed the successful integration of MIP and CQD, which created the selective lossy mode resonance (LMR) for DA monitoring. The experimental factors were optimized to obtain the maximum responses, and the sensing probe displays a dynamic response range of 0.3 to 100 $\mu$M and detection limit 0.027 $\mu$M. This strategy was successfully applied to detect DA in red wine, coffee, apple, orange, and broad bean juices samples, with negligible cross-reactivity toward other potential interfering species (e.g., Epinephrine, Ascorbic acid, Uric acid). This novel rotational optical fiber-based sensor has promising potential and versatility for point-of-care, portable, and on-site sensing of environmental and biological samples.**
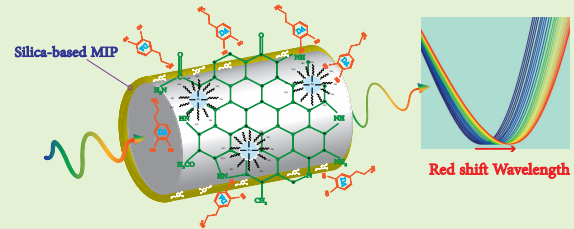
*Index Terms*— **Ratiometric Biosensors, Optical Fiber, Lossy Mode Resonance, Carbon Quantum Dot, Dopamine, Molecular Imprinting Polymer**

## I. INTRODUCTION

Dopamine (DA) is an important neurotransmitter in the brain and central nervous system that has a significant impact on mood, behavior, memory, attention, and movement, in addition to its role in transmitting information. A deficiency of DA can lead to neurological issues [1]. Recent studies have shown that DA may help in the treatment of Parkinson's and Alzheimer's diseases [2]. Therefore, quick and sensitive detection of DA is essential in modern medicine [1]. Various techniques such as fluorescence [3], electrochemistry [4], and photoelectrochemical [5] have been published for DA detection. However, these techniques are often complex, expensive, time-consuming, and require a large number of samples. Hence, there is a need to develop a sensitive and selective DA sensor. Recently, ratiometric sensors have become popular among researchers. While many ratiometric sensors use small fluorescent compounds, semiconductor quantum dots (QD) are more exciting due to their distinct optical and photophysical characteristics [6], [7]. Nanomaterials, such as QDs, have found extensive applications in different domains because of their compact dimensions and functional attributes. [8]. Carbon-based quantum dots (CQDs) are becoming increasingly popular due to their excellent photophysical properties, low toxicity, and low cost of synthesis [6]. A simple one-pot hydrothermal technique green approach [9] is used to synthesize CQDs with adjustable characteristics [10].

The fluorescence emission band of CQDs is adjustable, making them suitable for fluorescence resonance energy transfer ratiometry. The use of two independent fluorophores, such as CQDs and dye, or two CQDs, for ratiometry is enabled by broad excitation. The integration of fiber optics and nanoscience has resulted in the creation of bio-sensing systems that are practical, dependable, and capable of high selectivity and sensitivity [11]–[14]. Optical fiber sensors offer several advantages, including low cost, simplicity, resistance to electromagnetic interference and the ability to perform remote sensing [15]. Lossy mode resonance (LMR) occurs when light interacts with a waveguide coated with a film that has specific optical properties, resulting in a lossy mode and an absorption peak at a specific wavelength [16]. LMR differs from surface plasmon resonance (SPR) and can be supported by films made of various materials, such as metal oxide and polymers [17], [18]. One promising approach in sensor development involves combining sensors with Molecular Imprinting Polymer (MIP), which are synthetic polymers

T. Azargoshasb, H. Ali Navid, S. Yadollahzadeh, R. Aghbolaghi, are with the Department of Photonics, University of Bonab, Bonab, Iran (e-mail: tahereh.azargoshasb@gmail.com).
R. Parvizi is with the James Watt School of Engineering, University of Glasgow, Glasgow, U.K.
G-M. Parsanasab is with the Integrated Photonics Laboratory, Faculty of Electrical Engineering, Shahid Beheshti University, Tehran, Iran.
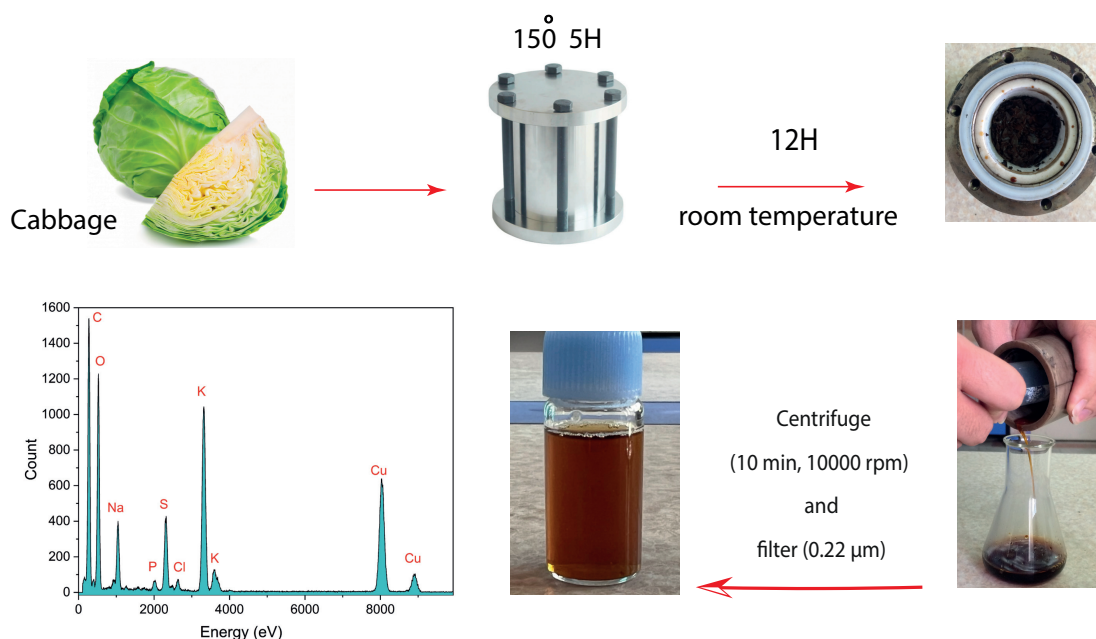
Fig. 1. A diagram illustrating the process of synthesizing blue-emitting carbon quantum dots from cabbage

with three-dimensional binding sites that have complementary structures to the target molecules they aim to detect [19], [20]. Silica-based MIPs synthesized in one pot are considered a straightforward technique in recent years [21], [22]. Overall, a molecular imprinting technique involves polymerizing a functional monomer and a cross-linker around a template molecule, resulting in the formation of three-dimensional cavities for specific recognition after the removal of the template molecule. MIPs can be created with specific sites for various templates, such as proteins, antibodies, enzymes, nucleic acids, viruses, bacteria, drugs, and so on, and they have advantages in terms of ease of synthesis, stability, and usability, making them highly suitable for the design of selective and sensitive analyte recognition sensors [23].

Our study aims to develop a new ratiometric fluorescence sensor for detecting DA by coating a silica-based MIP on cabbage-derived blue emissive carbon quantum dots (CQDs) and depositing them on an optical fiber [24], [25]. Very little is known about the use of a high-power ultrasonic probe in the synthesis of MIP. As a result, there is a strong desire to do more research on the production of MIP using this green technique. Herein, to detect samples, we constructed a novel form of CQDs/MIP using a simple and time-saving sol- gel polymerization technique. Cabbage was utilized to generate biomass CQDs utilizing a one- pot hydrothermal process without the use of complex preparatory techniques or harmful solvents. Because cabbage is employed as a carbon source, our method is low-cost, non-toxic, and environmentally beneficial. To the best of our knowledge, this is the first experimental demonstration of the LMR-based CQD-coated optical fiber ratiometric. We use a green synthesis approach that is cost-effective, environmentally friendly, and avoids the use of complex preparatory techniques or harmful solvents. This represents the first experimental validation of using LMR-

based CQD-coated optical fiber as ratiometric biosensors. To achieve specific detection, we use a sol-gel polymerization technique to create a unique form of CQDs/MIP. The optical fiber sensor is set up by mechanically removing a portion of the cladding from a multi-mode fiber's central section and immersing it in a CQDs/MIPs solution. The uniqueness of our research lies in the eco-friendly synthesis of highly luminescent CQDs and the innovative approach of grafting silica-based MIPs onto CQDs using ultrasonic irradiation. The resulting ratiometric MIP sensor showcases outstanding capabilities in terms of selectivity, stability, repeatability, and reliability, holding significant promise for a broad array of sensing applications.

## II. EXPERIMENTAL METHODS

### A. Materials and instruments

The following chemicals were acquired from Merck Co: Dopamine (DA), Glycine, hydrofluoric acid (HF 38-40%), hydrochloric acid (HCl), hydrogen peroxide ($H_2O_2$), sulfuric acid ($H_2SO_4$), (3-Aminopropyl) Triethoxysilane (APTES, 97%), and Tetraethyl orthosilicate (TEOS). Thorlabs Inc. supplied Plastic-cladding silica multi-mode fibers (PCS-MMFs) with a core/cladding diameter of 400/425 $\mu m$, specifically the FT400EMT variant. A local grocery store was the source of purchase for cabbage, which serves as a natural carbon source. The recording of Fourier transform infrared (FT-IR) spectra was performed using the Thermo Scientific Nicolet iS10 spectrometer, while a Mettler Toledo UV/Vis spectrophotometer UV7 was used for UV-VIS spectroscopy. The Agilent Technologies Cary Eclipse fluorescence spectrophotometer was utilized to acquire fluorescence spectra. The Tecnai G2 F20 transmission electron microscope, with an accelerating voltage of 200 $kV$, was employed to capture high-resolution transmission electron micrographs (HR-TEM). The
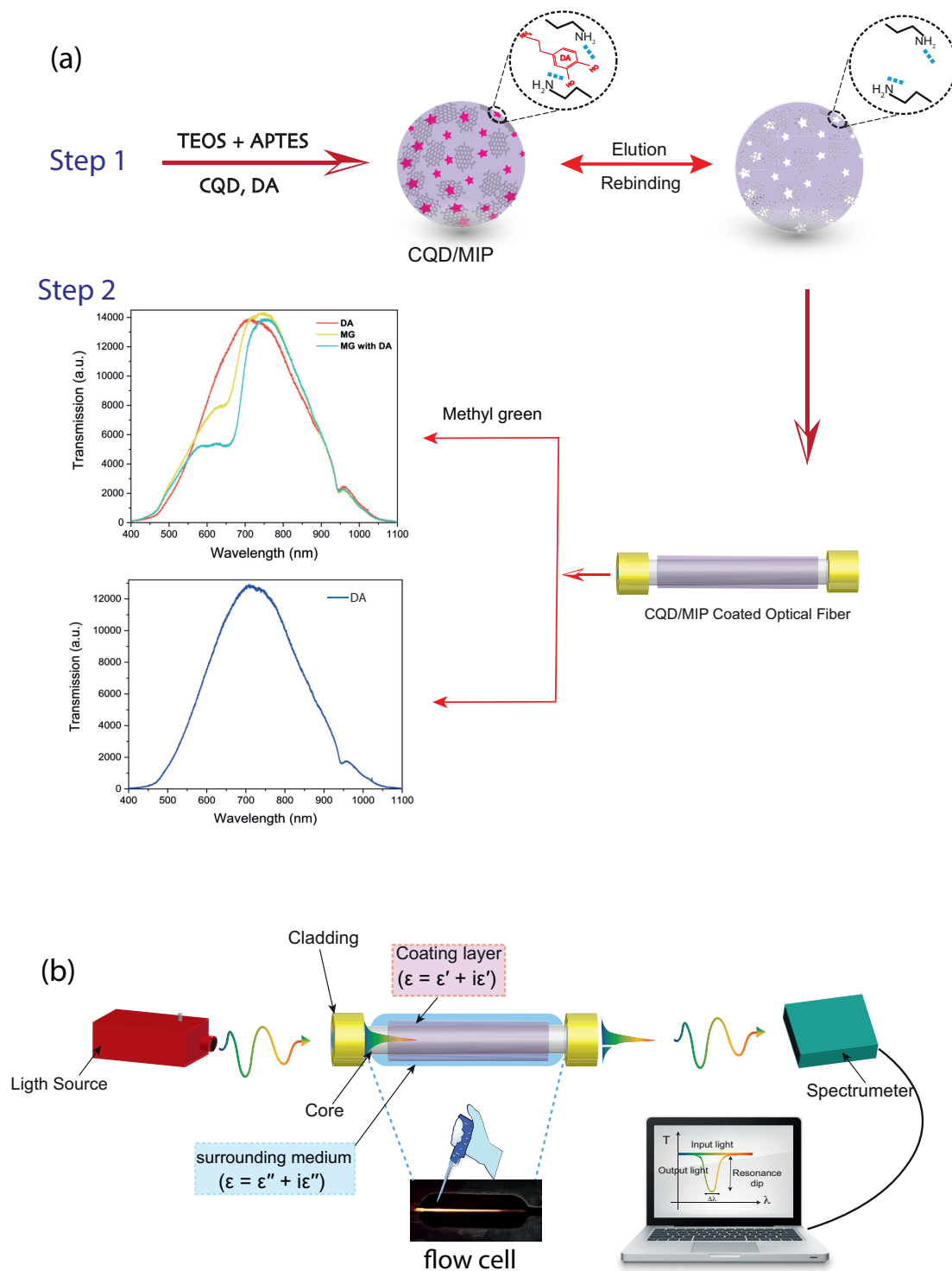
Fig. 2.  (a) The synthesis strategy and reaction mechanism for the specific binding and rebinding of the target analyte at the silica-based MIP layer coated optical fiber as ratiometric biosensors are illustrated in the schematic (b) The probe characterization was done using an experimental setup.

X-ray diffraction (XRD) pattern of the CDs was obtained by recording the diffraction of X-rays as they interacted with the CDs. This pattern provides information about the structure and composition of the CDs. The XRD analysis was performed using an X-Ray diffractometer, specifically the Philips PW 1730/10 model. The morphology and elemental composition of the sample were analyzed using field emission scanning electron microscopy (FE-SEM) with an energy-dispersive X-

ray analyzer (EDX). This technique involved capturing an image of the sample's surface using an SEM FEI Quanta 200, which was equipped with an EDX for elemental analysis. Raman spectra were obtained using a Raman microscope (Renishaw inVia). The experiments were conducted in an ultrasonic bath at a frequency of 20 $kHz$, with a continuous cycle lasting for 30 minutes.

## B. Green-CQDs preparation and characterization

We used a one-step green low-temperature carbonization method to create blue emissive CQDs using cabbage as the natural carbon source. We purchased a cabbage from a nearby store, cleaned it with distilled water, and chopped it into pieces for use in the hydrothermal reactor. The cabbage was put into a 50 $mL$ autoclave made of stainless steel and lined with Teflon, along with 15 mL of water, and heated to 150 C for 5 hours. The cooled dark brown solution was subjected to a 15-minute centrifugation at 11000 $rpm$ to separate the less-fluorescent bigger and any non-reactive CQDs. To remove large insoluble carbonaceous particles, the end product was filtered using a 0.22 $m$ membrane filter. The resulting supernatant of CQDs was then stored at 4°C for future characterization and sensor fabrication purposes. A diagram of the process can be found in Figure 1.

## C. Optical fiber surface functionalization

In order to form the sensing region of the Plastic Clad Silica (PCS) Multimode fiber-optics with core diameters of 400 $\mu m$ and refractive indices of $n_{core} = 1.458$ and $n_{clad} = 1.398$, a section of the cladding with a length of approximately 12 $mm$ was mechanically eliminated from the middle portion of the fiber. The fiber core was optimized by etching it with hydrofluoric acid for a specific period of time. Before immersing the fiber sample in a freshly prepared piranha solution (a mixture of concentrated sulfuric acid ($H_2SO_4$) and 15% hydrogen peroxide ($H_2O_2$)), it was washed twice with distilled water. The purpose of this process was to eliminate any organic impurities present in the fiber core, and the fiber remained in the piranha solution for 8 hours. As a result of the previous steps, the fiber surface became hydroxylated, making it suitable for interaction with the silane coupling agent APTES. Subsequently, the stripped fiber underwent a thorough cleaning process using deionized water and was completely dried.

## D. Preparation of CQDs/MIPs and CQDs/NIPs nano-composites coated probe

The general process to create CQDs/MIPs involves the following steps:

- **Preparation of the MIP:** This may involve the selection of the template molecule, functional monomers, cross-linkers, and initiators.
- **Polymerization:** The polymerization of the monomers in the presence of the template molecule to create the imprinted cavities.
- **Removal of the template:** After polymerization, the template molecule is removed, leaving behind the imprinted cavities.
- **Incorporation of CQDs:** The CQDs are incorporated into the MIP matrix, potentially through a surface-imprinting technique.
- **Characterization and application:** The prepared CQDs/MIPs are characterized for their selectivity, sensitivity, and stability, and then applied for specific detection purposes.

To produce blue emissive CQDs using cabbage, a green and low-temperature carbonization method was used during the synthesis process. A sol-gel process was employed to coat the CQDs with a silica-based molecular imprinting polymer (MIP). The synthesis of silica-based MIPs occurred in a single step after the preparation of the sensing region. To create the silica-based MIPs, APTES (a monomer with functional groups), TEOS (a cross-linker), and methanol were copoly-merized. A mixture of 0.7 mL of APTES, 1.5 mL of TEOS, and 10 mL of methanol was stirred for 30 minutes. To adjust the pH to 5-6, 0.5 mL of diluted hydrochloric acid was added. The solution obtained was agitated at ambient temperature for a duration of 10 minutes. The as-synthesized blue emissive CQDs were introduced into the solution, leading to the formation of nanocomposites of CQDs/MIP through sol-gel polymerization. The interaction between the CQDs and DA involved hydrogen bonding, facilitating the formation of the nanocomposites (Figure 2(a)). The optical fibers were submerged in the solution containing the nanocomposites, and an ultrasonic bath was utilized to ensure the nanoparticles were evenly distributed on the fibers. The DA molecules underwent several rounds of washing with acetic acid/ethanol to eliminate any molecules that were not bound or in excess (Figure 2(a)). After conducting multiple washing stages at 15-minute intervals, a careful optimization process determined that the best sensing performance was achieved after 1 hour. This duration effectively removed unwanted molecules. Furthermore,CQDs/NIPs were generated using the same procedure employed for creating the imprinted polymers (MIPs) on the CQDs, with the exception that DA was not added during the polymerization step. The experimental arrangement for the sensor's probe is illustrated in Figure 2(b).

## III. RESULTS AND DISCUSSION

### A. Characterization of the CQDs

The blue emissive carbon quantum dot (CQDs) derived from cabbage is composed of C, H, N, and O elements, which are present in various functional groups and are highly soluble in water. The following section provides a brief overview of the key features of green CQDs.

*1) Structural properties:* FT-IR transmittance spectra were utilized to detect surface functional groups on CQDs nanoparticles. The FT-IR spectra, as shown in Figure 3(a), indicate that these CQDs contain several hydrophilic groups, such as -OH, -COO-, and -NH, which make them highly soluble in water and enable them to act as biomolecule linkers. Additionally, UV-VIS spectra of CQDs have revealed the presence of many C=C and C=O conjugate structures. In the FT-IR spectrum, the absorption bands corresponding to the stretching vibrations of OH and NH are observed in the range of 3200-3500 $cm^{-1}$. Additionally, the band at 2930 $cm^{-1}$ signifies the stretching mode of C-H. The peaks at 1617 and 1102 $cm^{-1}$ have been attributed to C=C and N-H vibrations, respectively [26], [27]. The presence of carboxyl groups is indicated by the peaks at 1151 and 1021 $cm^{-1}$, which represent the stretching and bending vibrations of C-O bonds, respectively. Additionally, the peaks at 1652 and 1405 $cm^{-1}$ suggest the existence

This article has been accepted for publication in IEEE Sensors Journal. This is the author's version which has not been fully edited and content may change prior to final publication. Citation information: DOI 10.1109/JSEN.2023.3347262

T. AZARGOSHASB *et al.*: CARBON QUANTUM DOT OPTICAL FIBER BIOSENSORS TOWARD DOPAMINE DETECTION 5
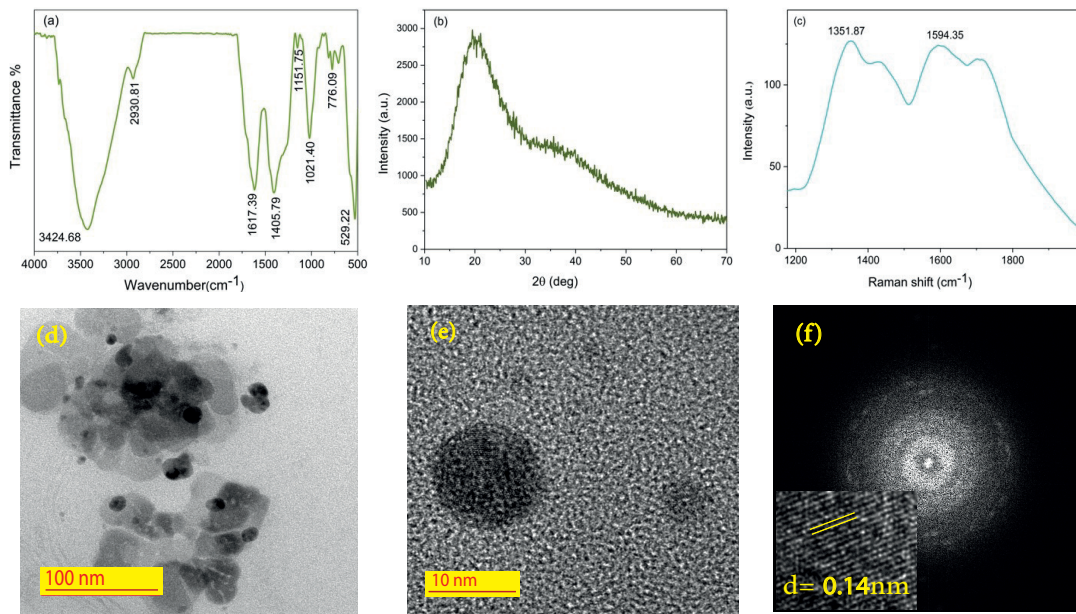
Fig. 3. (a) FT-IR spectrum, (b) XRD pattern, (c) Raman spectra and (d, e, f) HR-TEM images of the synthesized carbon dots
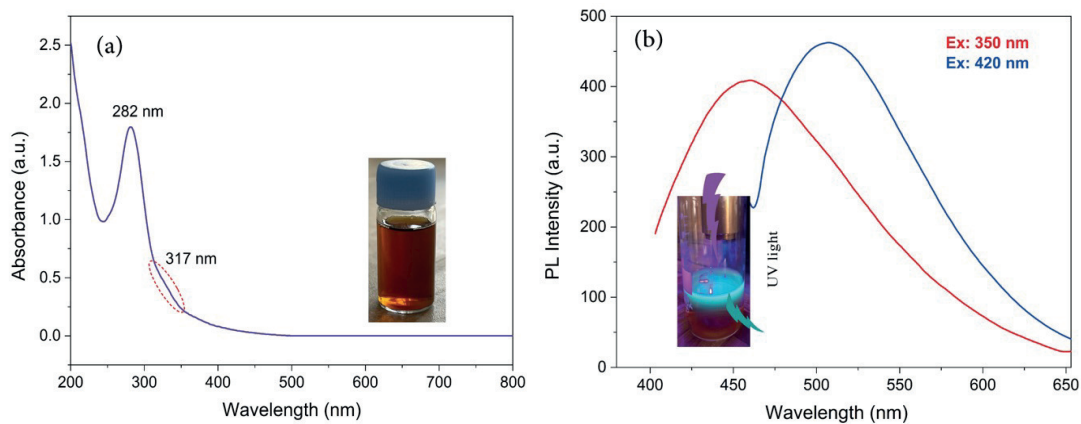


Fig. 4. (a) The UV-VIS absorption, (b) Photoluminescence intensity spectra at various excitation wavelengths of 350 and 420 $nm$, of the synthesized carbon dots

of C=O and COO- groups. The disordered arrangement of carbon atoms in CQDs powder often results in an amorphous character in their x-ray diffraction (XRD) pattern. Figure 3(b) illustrates the XRD pattern of CQDs. The XRD spectra of green CQDs typically exhibit a broad diffraction peak in the $2\theta$ range of 20°-25°, which corresponds to the (0 0 2) plane of mild graphitic nature, indicating the amorphous nature of CQDs [26], [28].

Raman spectroscopy is a powerful and non-destructive method for analyzing the lattice structure, electronic properties, optical properties, and phonon properties of carbon-based materials. The Raman spectra of the synthesized CQDs are shown in Figure 3(c). The D band, which represents $sp^3$ hybridized vibrations and indicates the degree of disorder in the material structure, was detected at 1351 $cm^{-1}$, while the G band, which represents $sp^2$ hybridized vibrations induced by well-structured CQDs, was found at 1611 $cm^{-1}$ [29]. The amorphous structure of the synthesized CQDs is supported by

both the XRD analysis (Figure 3(b)) and the Raman intensity ratio ($I_D/I_G$), which is calculated to be 1.02. The $I_D/I_G$ ratio, termed the intensity ratio of the D band to G band in Raman spectroscopy, is a significant parameter that indicates the presence of structural disorder and defects in carbon-based materials, especially the degree of crystallinity and relative abundance of carbon atoms as compared to surface toms [30]. To calculate the $I_D/I_G$ ratio from Raman studies, the following steps can be followed. First, obtain the Raman spectrum of the carbon-based material using a Raman spectrometer. Next, locate the positions of the D and G band peaks in the spectrum. If necessary, perform baseline subtraction to remove background signal and enhance visibility of the peaks. For more accurate results, fitting the D and G bands with Gaussian or Lorentzian functions may be required. After determining the positions and intensities of the bands, the $I_D/I_G$ ratio can be calculated using the formula: $I_D/I_G$ = (Intensity of D band)/(Intensity of G band) The intensities of the bands can
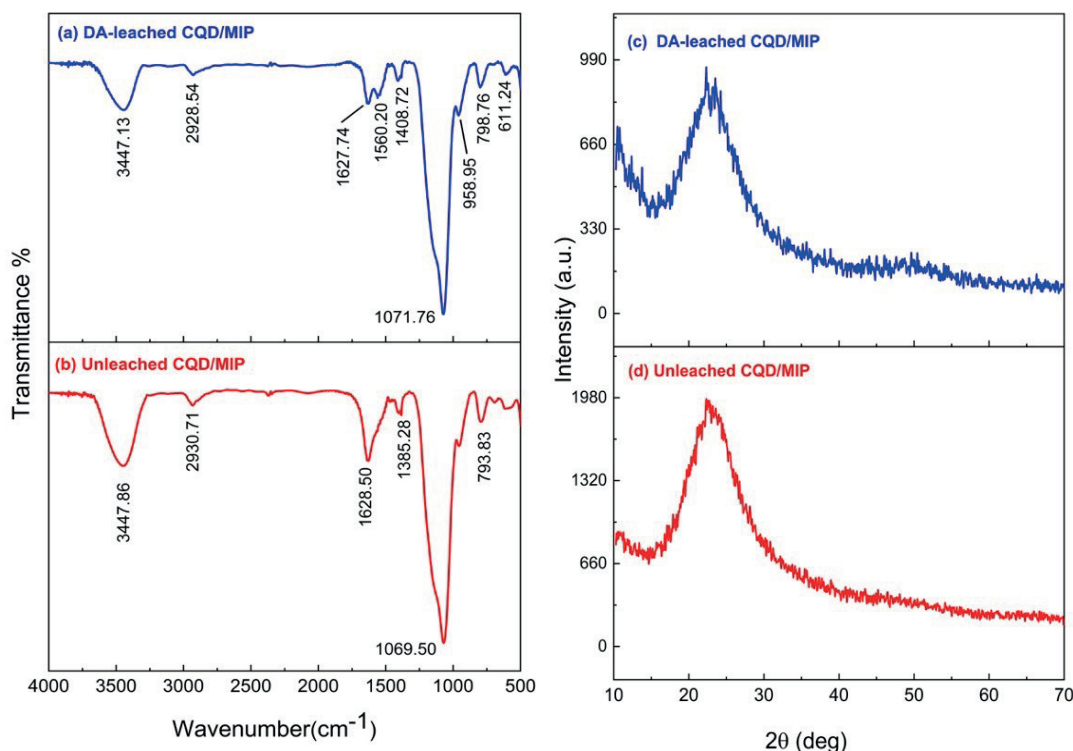
Fig. 5. The FT-IR spectrum and XRD pattern of the DA-leached CQDs/MIP and unleached DA CQDs/MIP are shown in (a,c) and (b,d) respectively.

be determined by integrating the area under each peak after fitting or using peak height, depending on the fitting method. This ratio provides valuable insights into the level of structural disorder and defects in the material. Figure 3(d-f) presents the results of the high-resolution transmission electron microscopy (HR-TEM) analysis, was used to examine the morphology and structures of CQDs extracted from cabbage. The HR-TEM images indicate that the particles were uniformly distributed and homogeneous, with a spherical morphology and an average diameter of less than 10 $nm$. The (1 0 0) in-plane lattice of graphite carbon was identified in the high-resolution transmission electron microscopy (HR-TEM) analysis, with a lattice fringe distance of 0.14 $nm$ (insets Figure 3(f)) [31]. The successful production of surface-functionalized CQDs derived from cabbage is confirmed by the EDX spectroscopy elemental mapping image, as shown in Figure 5.

*2) Optical properties:* UV-visible and photoluminescence spectrum analyses were performed to study the optical characteristics of CQDs. The aqueous solution of CQDs appears brown and clear in daylight but exhibits a bright blue-green fluorescence under UV light, which is visible to the naked eye (see insets Figure 4(a,b)). Figure 4(a) illustrates the absorption and emission spectra of the CQDs that were prepared. The absorption range of 230-285 $nm$ is commonly attributed to the $\pi - \pi^*$ transition of C=C and C=N bonds in carbon cores, which typically do not lead to fluorescence. Moreover, a secondary peak in the 300-330 $nm$ range is associated with the $\pi - \pi^*$ transition of C=O bonds.

During the partial carbonization of precursors, we observed that the absorption spectra extend to the visible region without any background absorption. This finding suggests that no other types of CQD nanocomposites are generated in the process [29]. This is described in Figure 4(b). The excitation wavelength dependence of the CQD's PL spectrum is also discussed in Figure 4(b). Excitation spectra were recorded at two excitation wavelengths ranging from 350 $nm$ to 420 $nm$. The photoluminescence spectrum demonstrates that the emission wavelength is influenced by the excitation wavelength. As the exciting wavelength increases, the emission peaks gradually intensify, suggesting that the emission wavelength can be modified by adjusting the excitation wavelength. The emission wavelength shifts towards the red end of the spectrum, and the emission intensity steadily rises as the excitation wavelength increases. This property, which is dependent on the excitation wavelength and could be beneficial in bioimaging applications, is possibly associated with the presence of surface energy trap distribution and diverse particle sizes [32].

### B. Characterization of the CQDs/NIPs and CQDs/MIPs nano-composites

The primary peaks of CQDs remain largely unchanged in Figure 3(a), indicating that the fundamental structures remained mostly similar after the addition of DA and did not un-dergo significant changes. The OH bond stretching is responsible for the broad peak observed at 3443 $cm^{-1}$, while the stretching vibration of C-H is the cause of the peak at 2924 $cm^{-1}$ [27]. Figure 5(a,b) displays two peaks associated with the C=C group and N-H group at the edge and surface of CQDs, respectively. These groups were produced through a sol-gel reaction between APTES and TEOS, indicating that the
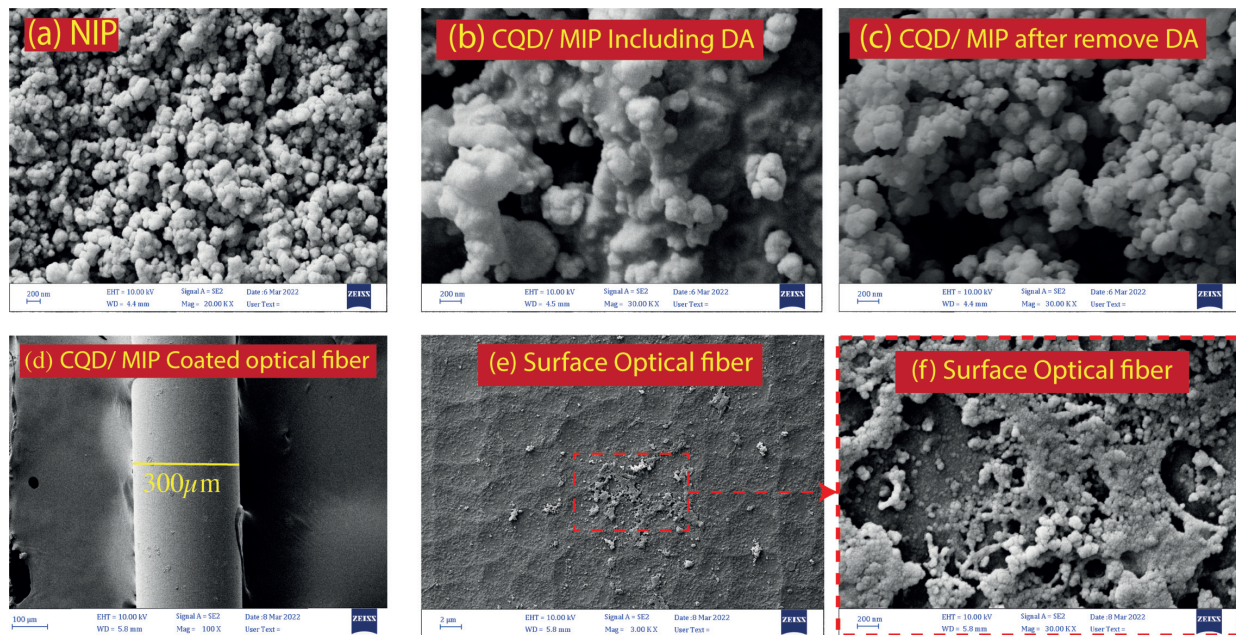
This article has been accepted for publication in IEEE Sensors Journal. This is the author's version which has not been fully edited and content may change prior to final publication. Citation information: DOI 10.1109/JSEN.2023.3347262

T. AZARGOSHASB *et al.*: CARBON QUANTUM DOT OPTICAL FIBER BIOSENSORS TOWARD DOPAMINE DETECTION
7

**Fig. 6.** The FE-SEM images of (a) NIP, (b) unleached, and (c) DA-leached CQDs/MIPs, as well as the (d,e) top view and (f) surface of CQDs/MIPs-coated optical fiber

produced CQDs/SiO$_2$ were amine-functionalized by APTES. The FT-IR spectra also revealed a significant peak at 1070 $cm^{-1}$, indicating silica polymerization (asymmetric stretching of Si-O-Si) [33]. The carboxyl group signal at 1560 $cm^{-1}$ was eliminated in spectrum Figure 5(a), suggesting that $NH^{+3}$ and COO- were likely formed due to the interaction between the amine group and the carboxylic group. The presence of the Si-O-Si stretching and bending vibrations, represented by the peaks at 958 $cm^{-1}$ and 798 $cm^{-1}$, respectively [27], [34], in addition to the characteristic peaks of CQDs, suggests the successful synthesis of imprinted polymers that incorporate CQDs/MIP. XRD analysis was utilized to determine the phase structure and crystalline nature of the silicasupported CQDs nanoparticles that were produced. Figure 5(c,d) displays the XRD graphs of DA-leached CQDs/MIPs and unleached CQDs/MIPs. The XRD patterns of both samples reveal a wide peak attributed to amorphous carbonaceous compounds, with no other distinguishing peak, confirming the presence of an amorphous structure in the core of CQDs. The characteristic peak observed at about 22.25°in the un-leached CQDs/MIPs corresponds to the (0 0 2) plane of the amorphous carbon network, which did not undergo significant changes after the removal of the target molecule. The presence of an amorphous structure can be attributed to the CQDs and the surface functional groups, specifically the SiO$_2$ shell layer that is formed through the use of APTES and TEOS [35].

Figure 6(a-f) display the Field Emission scanning electron micrographs (FE-SEM) of the non-imprinted polymer (NIP), unleached DA CQDs/MIPs, DA-leached CQDs/MIPs powder, DA-leached CQDs/MIPs coated fiber-optic, and the surface of CQDs/MIPs. The morphology and diameter of the sphere-shaped CQDs/MIPs and CQDs/NIPs nanocomposites are similar, with both having diameters of less than 100 $nm$. The surface of the nanocomposite is uniformly spherical

and rough. The surfaces of DA-leached CQDs/MIPs exhibit several specific imprinted cavities, while the FE-SEM images of CQDs/MIPs unleached DA show a smooth surface with no specific locations for target molecules in the nanocomposite structure. These results indicate that the analyte was effectively removed during the washing process, as evidenced by the porous structure in Figure 6(b,c). Additionally, the constituents of the nanocomposite powder were analyzed using EDX analyses. The CQDs/MIP and CQDs/NIP had essentially identical element types (Figure S3). The presence of Si and O confirms the existence of SiO$_2$ matrices produced by TEOS and APTES, while the amino group provided N in APTES. The average particle size of CQD/MIPs was greater than that of the CQDs, indicating that silica-based MIP was successfully coated on the CQDs.

## C. Basic concept of lossy-mode resonances and theoretical research of LMR-based sensors modified with CQDS/MIP layer

The sensitivity of an optical fiber evanescent-based sensor is determined by the strength and dispersion of the evanescent field in the surrounding medium [36], [37]. The evanescent wave is generated when light leaks from the core into the surrounding medium within the unclad region of the fiber, creating an evanescent field at the interface between the core and the surrounding medium. The amplitude of the evanescent wave decreases exponentially as it propagates from the core into the solution, indicating the presence of analyte molecules that have been adsorbed, attached, or bonded to the chemically treated surface of the fiber-optic. When a receptor molecule interacts with an analyte, it can be understood as a change in the mass of the coating layer on the fiber surface. This change in mass leads to a corresponding change in the refractive index of the coating layer. Assuming that the adsorbed molecules
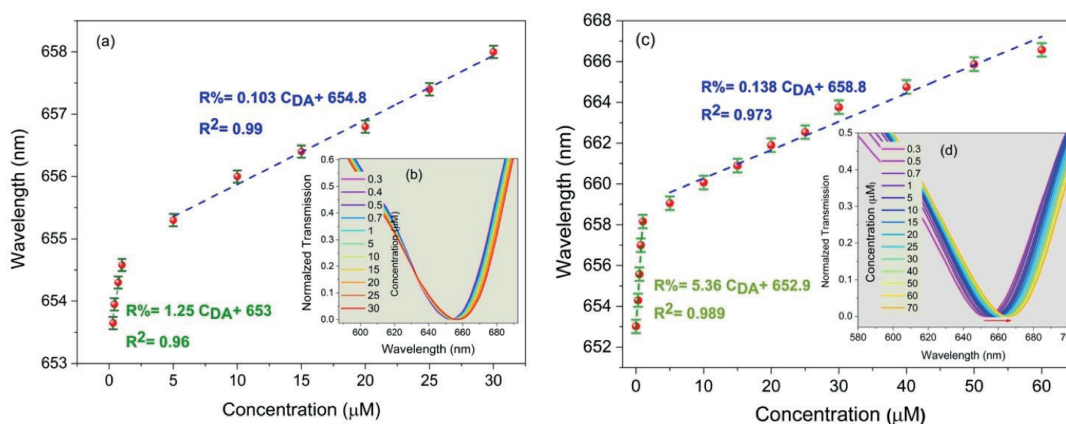
Fig. 7. The lossy mode resonance (LMR) shift for various DA concentrations: (a and b) 0.04 $g$ and (c and d) 0.08 $g$, was observed while keeping the concentration of CQD solution fixed at 12 $mL$.

form a homogeneous layer with a specific refractive index and thickness, the sensor's sensitivity is defined as the rate of change of the effective refractive index of the guided mode changes as the thickness of the adsorbed film changes [38]. To achieve high sensitivity, it is crucial to design the optical waveguide structure appropriately. The first step in obtaining a LMR is selecting a suitable thin-film material. The LMR phenomenon occurs when there is coupling between a waveguide mode and a particular lossy mode of a semiconductor thin film. This coupling requires a significant overlap between the mode fields, and a phase-matching condition where the real parts of the propagation constants are equal [39]. To achieve LMR, it is essential to determine the cutoff condition, which indicates the point where the mode begins to propagate through the coating. This condition is affected by two factors: the wavelength of the incident light and the thickness of the coating [17]. For specific wavelengths and characteristic thickness values, there is some weakening in the propagation of light. The shift in the wavelength of the LMR is primarily influenced by the real part of the refractive index, whereas the imaginary part of the refractive index determines the magnitude or depth of the LMR [40], [41].

## D. LMR-based sensing performance

To achieve optimal sensor performance, several variables need to be considered. The optimization of CQDs quantity and DA was performed to synthesize high-quality sensing probe CQDs/MIPs, and the layer thickness was adjusted by manipulating the synthesis time. This investigation involved three phases aimed at achieving optimal sensor performance while considering a constant environmental condition. The fluorescence detections were conducted under the same conditions. The broadband light source was adjusted between 360 and 2200 $nm$, and the sensing probe was placed in the flow cell. A precise amount of the as-prepared solution was added to the flow cell during the detection process. After that, the solution was allowed to sit for approximately 20 seconds to ensure complete interaction between the DA molecules and the silica-based MIP layer, and to reach stable conditions. After each measurement, ethanol and acetic acid were introduced

into the flow cell to wash and remove the analyte molecules. To determine the sensitivity of the sensor, the shift in the resonance wavelength ($\lambda_{res}$) is measured. This shift is directly related to changes in the refractive index difference between the guiding modes in the fiber core and the leaky evanescent waves in the coating of CQDs/MIPs surrounding the sensing medium. This dependency on refractive index is primarily attributed to the concentration of DA.

In this article, a ratiometric sensor was developed using two independent fluorophores, carbon quantum dots (CQDs) and a dye, to improve the sensor's performance. The CQDs can transfer energy and donate electrons to the dye molecules, facilitating the detection process. The presence of an analyte-binding agent, such as methyl green, in the sensing environment leads to a rapid response. To evaluate the effect of the dye on the sensor's results, different concentrations of DA were prepared using double distilled water. However, Figure 5(a) showed no significant changes in the signal with increasing concentrations of DA. Therefore, different concentrations of DA were prepared using a 30-ppm solution of methyl green. To eliminate any background effects before conducting the actual test, the probe was placed adjacent to the 30-ppm solution of the dye, and its spectrum was recorded. This process was then repeated for different concentrations of DA. The results, depicted in Figure S2 (b,c), show a decrease in the intensity of the transmission spectrum as the concentration of DA increases, along with a red-shift in the absorption wavelength. It was noticed that the wavelength of the LMR can be precisely adjusted by adjusting the concentrations of CQDs under identical conditions of duration and constant concentration of DA. The ability to adjust the LMR wavelength is a benefit of utilizing CQDs. To optimize the impact of carbon concentration, optical transmission spectra were obtained for different CQD concentrations (5, 10, 12, and 15 mL). The response obtained with 5 mL of CQDs was not satisfactory, so the concentration was increased. The results for the other concentrations were quite similar, and thus, the medium concentration (12 mL) was considered the optimal value. Additional details and supporting information can be found in Figure S3 of the accompanying document. Therefore, subsequent tests were conducted using 12 mL of CQDs.
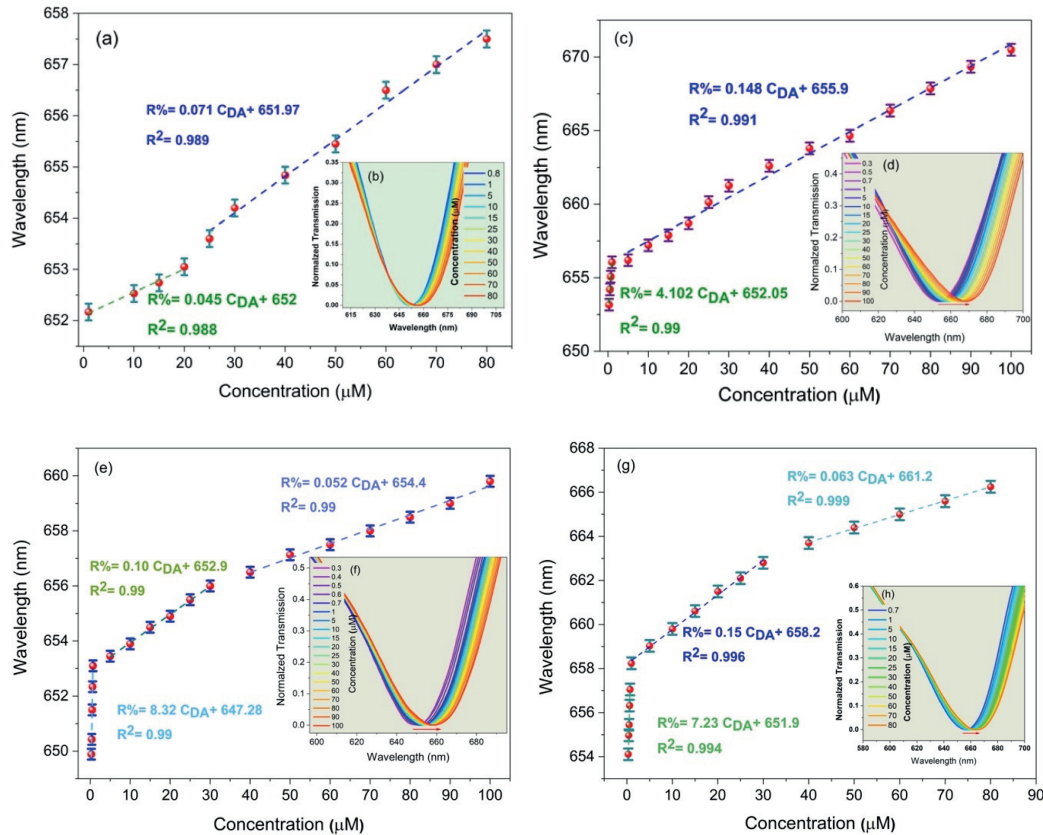
This article has been accepted for publication in IEEE Sensors Journal. This is the author's version which has not been fully edited and content may change prior to final publication. Citation information: DOI 10.1109/JSEN.2023.3347262

T. AZARGOSHASB *et al.*: CARBON QUANTUM DOT OPTICAL FIBER BIOSENSORS TOWARD DOPAMINE DETECTION 9



Fig. 8. The impact of the elapsed time on the LMR shift for (a,b) 3 h, (c,d) 5 h, (e,f) 6 h, and (g,h) 8 h.

*1) Optimizing the effect of the DA concentration:* To determine the quantity of imprinted target sites in the sensing region, the impact of changes in DA concentration was assessed while maintaining a constant concentration of 12 mL for the CQDs. The results show that when the CQD concentration (12 mL) and duration (4 hours) are fixed, an increase in the analyte (DA) concentration leads to an enhanced response of the sensing probe. Figure 7(a) and (b) illustrate that the sensitivity in the linear range is 1.25 $nm/M$ (0.1039 $nm/M$) for low (high) DA concentrations of 0.04 g. Moreover, when the DA concentration is 0.08 $g$, the sensitivity rises from 5.36 $nm/M$ at low concentrations to 0.138 $nm/M$ at high concentrations (as shown in Figure 7(c) and (d)). It is evident that with a constant CQD concentration, the sensitivity diminishes over a wider range of DA target molecule concentrations, which may be attributed to the memory effect of measuring the target molecule during successive tests. Moreover, as observed, the linear range of the sensing probe expands as the amount of analyte increases, likely due to an increase in the number of cavities formed on the surface of the sensing layer. It can be concluded that the increase in the effective refractive index of the sensor layer is responsible for the red-shift in $\lambda_{res}$ as a function of DA concentration. The red arrow in Figure 9(d) indicates that a higher concentration of DA can result in a steeper absorption profile, resulting in a more noticeable red-

shift in the transmission spectra. The response achieved its optimum level when the amount of DA in the solution reached 0.08 $g$. Therefore, subsequent studies used 12 $mL$ of CQDs and 0.08 $g$ of DA.

*2) Optimizing the effect of the deposition time under ultrasonic irradiation:* The sensing performance is directly impacted by the thickness of the sensing layer. Increasing the thickness of the sensing layer decreases the evanescent field, which affects the optimal sensing performance. Therefore, determining the ideal thickness of the silica-based MIP layer is crucial for achieving optimal results. Furthermore, to examine how the performance of the LMR-based optical fiber sensor is affected by the duration of immersion under ultrasound irradiation, the sensitivity was evaluated using a fixed concentration of 12 $mL$ for CQDs and 0.08 $g$ for DA. The fiber-optic was submerged in the reaction solution, and data were recorded at specific time intervals of 3, 4, 5, 6, and 8 hours from the start of the experiment. The results of this study are depicted in Figure 8(a-h) and Figure S7. While all test durations were able to detect DA, the results obtained after 5 hours of immersion time were superior to those of other timeframes. For durations exceeding 5 hours, the sensor's response exhibited linearity in three distinct regions. The thicknesses of the silica-based MIP layer can affect sensitivity by impeding rapid electron transport between CQDs and DA analytes. In the case of the sensor
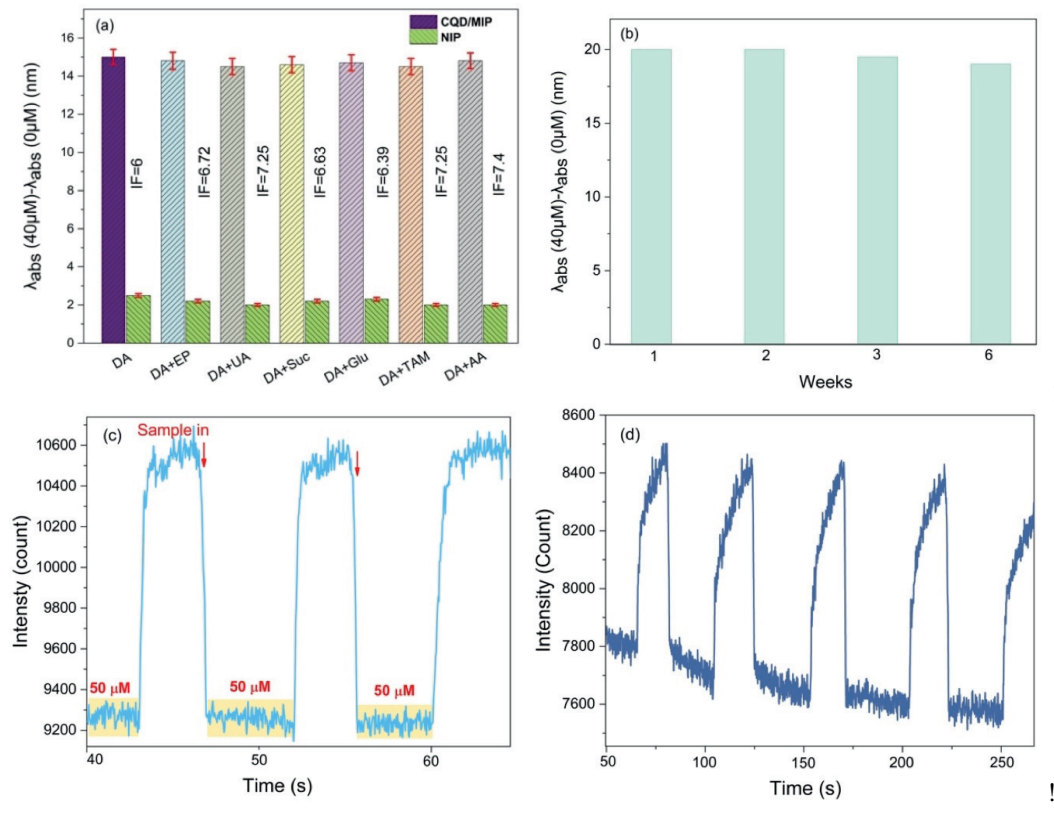
Fig. 9. (a) The selectivity responses of CQDs/MIP and CQDs/NIP nanocomposites, (b) stability plots, (c) and (d) dynamic diagram of probe under the optimized experimental conditions.

subjected to a 5-hour sol-gel process, it was observed that, in addition to expanding the measurement range (from 300 $nM$ to 100 $M$), the sensing probe demonstrated satisfactory linear response in both concentration regions.

### E. Selectivity of detection and applicability study

Under ideal experimental conditions, the selectivity of the CQDs/MIP (molecularly imprinted polymer) and CQDs/NIP (non-imprinted polymer) nanocomposites was investigated. The signal produced by DA (40 $\mu M$) was compared to other materials such as epinephrine, ascorbic acid, sucrose, uric acid, tamoxifen, and glucose in the presence of DA. The results showed that the CQDs/MIP nanocomposite exhibited remarkable identification impact and fluorescence quenching ability specifically for DA. In contrast, the selectivity of the CQDs/NIP nanocomposite was inferior (refer to Figure 9(a)). The high selectivity of CQDs/MIP is attributed to the cavities present on the surface of MIP-CQDs, which precisely match the form, size, and functional groups of DA [42]. To quantify the selectivity of the material, the imprinting factor (IF) was calculated using the formula IF = RMIP/RNIP [43]. The computed IF was 6, indicating that CQDs/MIP exhibits excellent selectivity in recognizing the analyte. The reusability of MIP sensors is crucial in empirical sensing applications and detection platform production. The proposed sensor was used for up to six weeks and yielded repeatable results. Although reduced sensitivity and selectivity may be observed

with repeated usage due to the regeneration of the imprinted cavity through washing the probe after each test and binding cycles, stability analysis revealed a negligible reduction in the shift compared to the initial reaction (as shown in Figure 9(b)). This indicates that the synthesized CQDs/MIP exhibited outstanding stability, as the fluorescence intensity did not significantly change over the course of six weeks under optimal conditions. Assessing the repeatability of MIP sensors is a crucial criterion to evaluate their performance. In this study, the dynamic behavior of the sensor was investigated to monitor variations in the output spectrum intensity. Figure 9(c,d) show the dynamic response of the probe when exposed to a solution. Initially, the intensity of the output spectrum was measured in a sample without the analyte. Then, the intensity spectra were recorded after introducing a 50 M sample into the flow cell. This process was repeated three times, with each measurement allowing the sample to remain in the probe area. Furthermore, Figure 9(d) demonstrates the dynamic response of the sensor to different analyte concentrations in the surrounding medium. It is evident that increasing the analyte concentration results in intensity changes, highlighting the rapid response capability of the sensor.

### F. Real sample analysis

The accuracy of an analytical technique depends on its ability to analyze real samples correctly. Regarding the proposed optical fiber sensor based on LMR, it was used to measure

This article has been accepted for publication in IEEE Sensors Journal. This is the author's version which has not been fully edited and content may change prior to final publication. Citation information: DOI 10.1109/JSEN.2023.3347262

T. AZARGOSHASB *et al.*: CARBON QUANTUM DOT OPTICAL FIBER BIOSENSORS TOWARD DOPAMINE DETECTION 11

TABLE I

COMPARISON OF THE PRESENTED METHOD WITH OTHER REPORTED METHODS FOR DETERMINING DOPAMINE.

| Method | Material | Linear concentration range($\mu M$) | LOD ($\mu M$) | Reference |
|---|---|---|---|---|
| Electrochemical | RGO/MWCNT/PTA/GCE | 0.5-20 | 1.14 | [44] |
| Electrochemical | MnO2/MWCNT/EPGC | 1-50 | 0.8 | [45] |
| LSPR | Ag Nanoparticles | 0–1 | 0.06 | [46] |
| Electrochemical | MIPs/pThi/NPG | 0.3–100 | 0.1 | [47] |
| Potentiometric | DA-MIP | 5-80 | 2.1 | [48] |
| **LMR** | **MIP/Carbon Quantum Dot** | **0.3-1** **1-100** | **0.027** | **This work** |

the DA analyte in various juice, coffee, and red wine samples. The samples were diluted ten times and transferred to the flow cell before analysis. Drug-free juices were used as reference samples. The sensor did not detect any DA in these samples. To assess recovery, the samples were spiked with different concentrations of standard DA. Various concentrations of the standard solution were added to the sample solutions to determine the optical response of DA. The results showed satisfactory recovery rates ranging from 94% to 103% for DA. These results demonstrate the successful application of the proposed approach in analyzing real samples. Hence, it is clear that the potential of the suggested sensor for detecting DA in actual samples is considerable.

### G. Comparison of the fabricated optical nano-sensor with other methods reported for dopamine detection

When evaluating the ability of an analytical method to detect analytes at very low concentrations, it is crucial to consider the limit of detection (LOD).To determine the limit of detection (LOD), the formula LOD = 3.3 $(S_y/S)$ can be utilized, where $S_y$ is the standard deviation of the response curve, and $S$ is the slope of the calibration curve. In this study, the LOD was determined using optimized sensor probes obtained through a 5-hour sol-gel procedure, with 12 $mL$ of CQDs and 0.08 $g$ of DA. The calculated LOD was as low as 0.03 $\mu M$. To compare the performance of the suggested approach with previously published methods for dopamine detection, linear range of various methodologies and detection limit are shown in Table I. Our proposed biosensor demonstrates a satisfactory detection limit and linear range when compared to prior research. This approach is considered effective due to its notable characteristics such as a low detection limit, adequate linear range, cost-effectiveness, and eco-friendliness.

### IV. CONCLUSIONS

To summarize, we have successfully developed an LMR-based rotational optical fiber sensor for measuring dopamine levels. This sensor uses CQDs/MIP nanocomposites coated on the uncladding optical fiber. It is the initial experimental demonstration of an LMR-based CQDs-coated fiber-optic ratiometric sensor specifically designed for dopamine detection. The cabbage-derived blue emissive CQDs were characterized using XRD, UV-VIS, FT-IR, and HR-TEM spectroscopic analyses. The fluorescence emission mechanism of the CQDs

was also investigated. After modifying the CQDs with silica-based MIPs using a direct ultrasonic irradiation technique, they were integrated into the optical fiber sensor. The sensor operates based on the wavelength shift of the transmission spectrum dip. Under optimized conditions, it demonstrates a sensitivity of 0.37 $nm/M$, enabling the detection of dopamine at low concentrations with a LOD achieved at 0.027 $\mu M$. The sensor exhibits excellent recoveries of up to 103% and demonstrates a high imprinting factor of 6, highlighting its selectivity for dopamine detection in aqueous samples. The sensor's sensitivity behavior is linear, which is highly desirable for practical applications. Based on the results obtained, CQD/MIP sensors prove to be suitable for rapid and precise measurements of dopamine in real aqueous samples. Consequently, the developed fiber-optic sensor holds great promise for monitoring chemical processes and finding diverse applications in biomedical and industrial settings.

### SUPPORTING INFORMATION

The Supporting Information is available free of charge.

- **S1**: EDX spectrum of carbon dot nanoparticles
- **S2**: Diffuse reflectance spectra (DRS) and Tuce plot
- **S3**: Mapping image and EDX spectrum of CQDs/MIP nanocomposite
- **S4**: Transmission spectra
- **S5**: The results of the recovery and accuracy test for real sample analysis under the optimal experience conditions

### DECLARATIONS

The authors declare no conflicts of interest.

### REFERENCES

[1] J. Ahmed, M. Faisal, F. A. Harraz, M. Jalalah, and S. Alsareii, "Development of an amperometric biosensor for dopamine using novel mesoporous silicon nanoparticles fabricated via a facile stain etching approach," *Physica E: Low-dimensional Systems and Nanostructures*, vol. 135, p. 114952, 2022.

[2] A. Roychoudhury, S. Basu, and S. K. Jha, "Dopamine biosensor based on surface functionalized nanostructured nickel oxide platform," *Biosensors and Bioelectronics*, vol. 84, pp. 72–81, 2016.

[3] S. Kruss, D. P. Salem, L. Vuković, B. Lima, E. Vander Ende, E. S. Boyden, and M. S. Strano, "High-resolution imaging of cellular dopamine efflux using a fluorescent nanosensor array," *Proceedings of the National Academy of Sciences*, vol. 114, no. 8, pp. 1789–1794, 2017.

[4] H. Yang, C. Zhou, J. An, L. Yang, Y. Yang, and X. Liu, "Ultra-fast synthesis of iron decorated multiwalled carbon nanotube composite materials: A sensitive electrochemical sensor for determining dopamine," *Journal of Alloys and Compounds*, vol. 897, p. 163257, 2022.

[5] K. Dashtian, S. Hajati, and M. Ghaedi, "Ti-based solid-state imprinted-cu2o/cuinse2 heterojunction photoelectrochemical platform for highly selective dopamine monitoring," *Sensors and Actuators B: Chemical*, vol. 326, p. 128824, 2021.

[6] Y. Han, W. Yang, X. Luo, X. He, H. Zhao, W. Tang, T. Yue, and Z. Li, "Carbon dots based ratiometric fluorescent sensing platform for food safety," *Critical Reviews in Food Science and Nutrition*, vol. 62, no. 1, pp. 244–260, 2022.

[7] D. Kumar, C. M. S. Negi, S. K. Gupta, and J. Kumar, "Effect of shape anisotropy and size on the electronic structure of cdse/znse quantum dots," *IEEE transactions on nanotechnology*, vol. 12, no. 6, pp. 925–930, 2013.

[8] R. Prasad, *Plant Nanobionics: Volume 2, Approaches in Nanoparticles, Biosynthesis, and Toxicity*. Springer, 2019.

[9] Z. Wang, L. Cao, Y. Ding, R. Shi, X. Wang, H. Lu, Z. Liu, F. Xiu, J. Liu, and W. Huang, "One-step and green synthesis of nitrogen-doped carbon quantum dots for multifunctional electronics," *RSC advances*, vol. 7, no. 35, pp. 21 969–21 973, 2017.

[10] V. Raikwar, "Synthesis and study of carbon quantum dots (cqds) for enhancement of luminescence intensity of cqd@ lapo4: Eu3+ nanocomposite," *Materials Chemistry and Physics*, vol. 275, p. 125277, 2022.

[11] A. Paliwal, A. Sharma, M. Tomar, and V. Gupta, "Carbon monoxide (co) optical gas sensor based on zno thin films," *Sensors and Actuators B: Chemical*, vol. 250, pp. 679–685, 2017.

[12] R. Pravesh, D. Kumar, B. P. Pandey, V. S. Chaudhary, D. Singh, and S. Kumar, "Advanced refractive index sensor based on photonic crystal fiber with elliptically split cores," *Optical and Quantum Electronics*, vol. 55, no. 13, p. 1205, 2023.

[13] V. S. Chaudhary, D. Kumar, B. P. Pandey, and S. Kumar, "Advances in photonic crystal fiber-based sensor for detection of physical and biochemical parameters-a review," *IEEE Sensors Journal*, 2022.

[14] V. S. Chaudhary, D. Kumar, and S. Kumar, "Au-tio 2 coated photonic crystal fiber based spr refractometric sensor for detection of cancerous cells," *IEEE Transactions on NanoBioscience*, 2022.

[15] S. Lépinay, A. Ianoul, and J. Albert, "Molecular imprinted polymer-coated optical fiber sensor for the identification of low molecular weight molecules," *Talanta*, vol. 128, pp. 401–407, 2014.

[16] S. Sharma, A. M. Shrivastav, and B. D. Gupta, "Lossy mode resonance based fiber optic creatinine sensor fabricated using molecular imprinting over nanocomposite of mos 2/sno 2," *IEEE Sensors Journal*, vol. 20, no. 8, pp. 4251–4259, 2020.

[17] Q. Wang and W.-M. Zhao, "A comprehensive review of lossy mode resonance-based fiber optic sensors," *Optics and Lasers in Engineering*, vol. 100, pp. 47–60, 2018.

[18] F. Chiavaioli and D. Janner, "Fiber optic sensing with lossy mode resonances: Applications and perspectives," *Journal of Lightwave Technology*, vol. 39, no. 12, pp. 3855–3870, 2021.

[19] A. Karrat, A. Lamaoui, A. Amine, J. M. Palacios-Santander, and L. Cubillana-Aguilera, "Applications of chitosan in molecularly and ion imprinted polymers," *Chemistry Africa*, vol. 3, pp. 513–533, 2020.

[20] A. Lamaoui, J. J. García-Guzmán, A. Amine, J. M. Palacios-Santander, and L. Cubillana-Aguilera, "Synthesis techniques of molecularly imprinted polymer composites," in *Molecularly Imprinted Polymer Composites*. Elsevier, 2021, pp. 49–91.

[21] H. Gholami, M. Ghaedi, A. Ostovan, M. Arabi, and A. R. Bagheri, "Preparation of hollow porous molecularly imprinted and aluminum (iii) doped silica nanospheres for extraction of the drugs valsartan and losartan prior to their quantitation by hplc," *Microchimica Acta*, vol. 186, pp. 1–9, 2019.

[22] D. Xiao, L. Su, Y. Teng, J. Hao, and Y. Bi, "Fluorescent nanomaterials combined with molecular imprinting polymer: synthesis, analytical applications, and challenges," *Microchimica Acta*, vol. 187, pp. 1–15, 2020.

[23] Y. Saylan, S. Akgönüllü, H. Yavuz, S. Ünal, and A. Denizli, "Molecularly imprinted polymer based sensors for medical applications," *Sensors*, vol. 19, no. 6, p. 1279, 2019.

[24] N. B. Messaoud, A. A. Lahcen, C. Dridi, and A. Amine, "Ultrasound assisted magnetic imprinted polymer combined sensor based on carbon black and gold nanoparticles for selective and sensitive electrochemical detection of bisphenol a," *Sensors and Actuators B: Chemical*, vol. 276, pp. 304–312, 2018.

[25] A. Lamaoui, J. M. Palacios-Santander, A. Amine, and L. Cubillana-Aguilera, "Computational approach and ultrasound probe–assisted synthesis of magnetic molecularly imprinted polymer for the electrochemical detection of bisphenol a," *Materials Science and Engineering: B*, vol. 277, p. 115568, 2022.

[26] Z. Li, Q. Wang, Z. Zhou, S. Zhao, S. Zhong, L. Xu, Y. Gao, and X. Cui, "Green synthesis of carbon quantum dots from corn stalk shell by hydrothermal approach in near-critical water and applications in detecting and bioimaging," *Microchemical Journal*, vol. 166, p. 106250, 2021.

[27] N. Kazemifard, A. A. Ensafi, and B. Rezaei, "Green synthesized carbon dots embedded in silica molecularly imprinted polymers, characterization and application as a rapid and selective fluorimetric sensor for determination of thiabendazole in juices," *Food chemistry*, vol. 310, p. 125812, 2020.

[28] K. Nekoueian, M. Amiri, M. Sillanpää, F. Marken, R. Boukherroub, and S. Szunerits, "Carbon-based quantum particles: an electroanalytical and biomedical perspective," *Chemical Society Reviews*, vol. 48, no. 15, pp. 4281–4316, 2019.

[29] P. Kumar, S. Dua, R. Kaur, M. Kumar, and G. Bhatt, "A review on advancements in carbon quantum dots and their application in photovoltaics," *RSC advances*, vol. 12, no. 8, pp. 4714–4759, 2022.

[30] X. Zhang, J. Wang, J. Liu, J. Wu, H. Chen, and H. Bi, "Design and preparation of a ternary composite of graphene oxide/carbon dots/polypyrrole for supercapacitor application: Importance and unique role of carbon dots," *Carbon*, vol. 115, pp. 134–146, 2017.

[31] W. Liu, G. Huang, X. Su, S. Li, Q. Wang, Y. Zhao, Y. Liu, J. Luo, Y. Li, C. Li *et al.*, "Zebrafish: a promising model for evaluating the toxicity of carbon dot-based nanomaterials," *ACS Applied Materials & Interfaces*, vol. 12, no. 43, pp. 49 012–49 020, 2020.

[32] G. Chellasamy, S. K. Arumugasamy, S. Govindaraju, and K. Yun, "Green synthesized carbon quantum dots from maple tree leaves for biosensing of cesium and electrocatalytic oxidation of glycerol," *Chemosphere*, vol. 287, p. 131915, 2022.

[33] H. Liu, L. Ding, L. Chen, Y. Chen, T. Zhou, H. Li, Y. Xu, L. Zhao, and N. Huang, "A facile, green synthesis of biomass carbon dots coupled with molecularly imprinted polymers for highly selective detection of oxytetracycline," *Journal of industrial and engineering chemistry*, vol. 69, pp. 455–463, 2019.

[34] J.-J. You, H. Liu, R.-R. Zhang, Q.-F. Pan, A.-L. Sun, Z.-M. Zhang, and X.-Z. Shi, "Development and application of tricolor ratiometric fluorescence sensor based on molecularly imprinted nanoparticles for visual detection of dibutyl phthalate in seawater and fish samples," *Science of The Total Environment*, vol. 848, p. 157675, 2022.

[35] B. Ramezanzadeh, E. Ghasemi, M. Mahdavian, E. Changizi, and M. M. Moghadam, "Characterization of covalently-grafted polyisocyanate chains onto graphene oxide for polyurethane composites with improved mechanical properties," *Chemical Engineering Journal*, vol. 281, pp. 869–883, 2015.

[36] K. Tiefenthaler and W. Lukosz, "Sensitivity of grating couplers as integrated-optical chemical sensors," *JOSA B*, vol. 6, no. 2, pp. 209–220, 1989.

[37] O. Parriaux and G. Veldhuis, "Normalized analysis for the sensitivity optimization of integrated optical evanescent-wave sensors," *Journal of lightwave technology*, vol. 16, no. 4, p. 573, 1998.

[38] F. Prieto, A. Llobera, A. Calle, L. M. Lechuga *et al.*, "Design and analysis of silicon antiresonant reflecting optical waveguides for evanscent field sensor," *Journal of lightwave technology*, vol. 18, no. 7, p. 966, 2000.

[39] I. Del Villar, C. R. Zamarreño, M. Hernaez, F. J. Arregui, and I. R. Matias, "Lossy mode resonance generation with indium-tin-oxide-coated optical fibers for sensing applications," *Journal of Lightwave Technology*, vol. 28, no. 1, pp. 111–117, 2010.

[40] I. Del Villar, M. Hernaez, C. R. Zamarreño, P. Sánchez, C. Fernández-Valdivielso, F. J. Arregui, and I. R. Matias, "Design rules for lossy mode resonance based sensors," *Applied optics*, vol. 51, no. 19, pp. 4298–4307, 2012.

[41] J. M. Corres, I. Del Villar, F. J. Arregui, and I. R. Matias, "Analysis of lossy mode resonances on thin-film coated cladding removed plastic fiber," *Optics letters*, vol. 40, no. 21, pp. 4867–4870, 2015.

[42] A. A. Ensafi, N. Kazemifard, and B. Rezaei, "Development of a selective prilocaine optical sensor based on molecularly imprinted shell on cdte quantum dots," *Sensors and Actuators B: Chemical*, vol. 242, pp. 835–841, 2017.

[43] T. Azargoshasb, H. A. Navid, R. Parvizi, and H. Heidari, "Evanescent wave optical trapping and sensing on polymer optical fibers for ultra-trace detection of glucose," *ACS omega*, vol. 5, no. 35, pp. 22 046–22 056, 2020.

[44] Y.-Y. Ling, Q.-A. Huang, M.-S. Zhu, D.-X. Feng, X.-Z. Li, and Y. Wei, "A facile one-step electrochemical fabrication of reduced graphene oxide–mutilwall carbon nanotubes–phospotungstic acid composite for

dopamine sensing," *Journal of Electroanalytical Chemistry*, vol. 693, pp. 9–15, 2013.

[45] Y. Wang, L. Wang, and Q. Zhuang, "A ratiometric electrochemical sensor for dopamine detection based on hierarchical manganese dioxide nanoflower/multiwalled carbon nanotube nanocomposite modified glassy carbon electrode," *Journal of Alloys and Compounds*, vol. 802, pp. 326–334, 2019.

[46] Y. Lin, C. Chen, C. Wang, F. Pu, J. Ren, and X. Qu, "Silver nanoprobe for sensitive and selective colorimetric detection of dopamine via robust ag–catechol interaction," *Chemical Communications*, vol. 47, no. 4, pp. 1181–1183, 2011.

[47] J. Yang, Y. Hu, and Y. Li, "Molecularly imprinted polymer-decorated signal on-off ratiometric electrochemical sensor for selective and robust dopamine detection," *Biosensors and Bioelectronics*, vol. 135, pp. 224–230, 2019.

[48] C. Wang, L. Qi, and R. Liang, "A molecularly imprinted polymer-based potentiometric sensor based on covalent recognition for the determination of dopamine," *Analytical Methods*, vol. 13, no. 5, pp. 620–625, 2021.